metrology

Article

Wheelset Wear Condition Evaluation Based on High-Precision Online Measurement of Geometric Parameters

Saisai Liu [1,2], Qixin He [1,2], Wenjie Fu [1,2], Qiang Han [3] and Qibo Feng [1,2,*]

1 School of Physical Science and Engineering, Beijing Jiaotong University, Beijing 100044, China
2 Ministry of Education Key Laboratory of Luminescence and Optical Information, Beijing Jiaotong University, Beijing 100044, China
3 Infrastructure Inspection Research Institute, China Academy of Railway Sciences Corporation Limited, Beijing 100081, China
* Correspondence: qbfeng@bjtu.edu.cn; Tel.: +86-010-51685558

Abstract

Train wheel wear is a critical factor affecting train operational safety, making the accurate and objective evaluation of wheel wear condition essential. However, current approaches are still constrained by inadequate measurement accuracy and incomplete evaluation methods. To address this issue, this study proposes an integrated method for the high-precision measurement and wear condition evaluation of train wheels. A multi-sensor data fusion-based measurement method is developed to synchronously acquire key wear-related parameters, including wheel diameter, flange height, and flange thickness. Based on the measured data, a matter-element model combined with game-theoretic weighting is established to evaluate wheel wear condition. Experimental results show that the proposed online measurement method for in-service wheels achieves standard deviations below 0.15 mm, and the measurement errors satisfy the requirements of Chinese railway industry standards. The evaluation results derived from the high-precision measurement data indicate that wheel wear condition gradually deteriorates with increasing service mileage, and that flange height wear is the dominant factor affecting the wear grade. These findings are consistent with actual operating conditions. The proposed method integrates high-precision multi-parameter measurements with wear condition evaluation, providing a reliable technical basis for wheel condition monitoring and predictive maintenance in rail transit.

Keywords: wheel wear measurement; wear condition evaluation; multi-dimensional sensors fusion; matter-element evaluation model; train wheel wear

1. Introduction

As the core load-bearing component connecting trains and tracks, the wear condition of wheels directly determines the safety, stability, and comfort of train operation. Excessive wheel wear will aggravate wheel–rail contact fatigue and even cause serious safety accidents such as derailment. Therefore, the accurate evaluation of wheel wear condition is of great importance for train operation safety, which requires the evaluation model to be effective and accurate, and in turn relies on high-precision wear measurement data as the support. Thus, effective, accurate evaluation and high-precision measurement are both key research directions in the fields of railway transportation and metrology [1–3].

For the accurate evaluation of wheel wear, the effectiveness and accuracy of the evaluation model are critical. Existing research on wheel wear condition evaluation typically relies

Received: 13 March 2026
Revised: 20 April 2026
Accepted: 5 May 2026
Published: 8 May 2026

on threshold judgments based on a single indicator such as diameter or flange thickness, which lacks comprehensiveness [4]. Therefore, comprehensive evaluation of wheel wear condition, which reflects the complex wear process of wheels, has gradually become a research direction. Wang et al. [5,6] defined the hunting coefficient (HC) from wheelset signals, established its hunting performance thresholds through simulation, and showed through field application that HC effectively identifies hunting instability in freight wagons, thus enabling evaluation of suspension parameters. Dai et al. [7] proposed a stacking feature deep forest model to predict hunting instability from wheel/rail contact parameters, achieved 85% accuracy in binary classification, and identified equivalent conicity of 1 mm as the key factor. In contrast to the studies on wheel/rail contact performance discussed above, the matter-element evaluation method has been widely developed as a multi-indicator comprehensive evaluation tool. It exhibits significant advantages in multi-indicator comprehensive evaluation [8–10], and has been maturely applied in many fields such as rail transit [11–13], civil engineering [14], geotechnical engineering [15], and hydraulic engineering [16]. The matter-element evaluation method is used to handle the fuzziness and uncertainty in the evaluation process, making the evaluation results more intuitive and reliable. Yi et al. [11] constructed a catenary condition evaluation model, using the matter-element model to determine the catenary condition grade, in which EWM and AHP were used to determine the indicator weights. Peng et al. [17] constructed a rail transit planning scheme based on the matter-element model, in which subjective and objective weights were used for comprehensive weighting of evaluation indicators. Because wheel wear is a complex and uncertain process, comprehensive evaluation of the wear condition using multiple indicators such as wheel diameter, flange height, and flange thickness remains a challenging problem [18]. In this work, we introduce the matter-element model for a comprehensive evaluation of wheel wear. This model enables accurate determination and quantitative description of the wear condition by means of classical domains, extended domains, and correlation functions, showing strong adaptability and good engineering practicality in multi-indicator comprehensive evaluation.

On the other hand, the accuracy of evaluation results depends entirely on the quality of measurement data, which means high-precision wheel wear measurement is the prerequisite for effective and accurate evaluation. Ran et al. [19] proposed a wheel profile parameter measurement method based on line-structured light vision sensing, and designed a targeted sub-pixel stripe center extraction algorithm to achieve fast and accurate measurement of wheel profiles. Pan et al. [20] adopted two sets of line-structured light vision sensors for data compensation, improving the stability of profile measurements. Zheng et al. [21] constructed an on-line wheel diameter measurement system based on the three-point method. However, existing studies typically measure wheel diameter and profile parameters separately without fully accounting for the coupling errors that occur during online measurement [22]. In diameter measurement, positioning errors cause the measured value to deviate from the defined rolling circle diameter, leading to systematic measurement errors. In profile parameter measurement using structured light vision, the eccentricity error caused by dynamic changes in wheel diameter is often neglected. These two types of errors interact with each other, and a single type of sensor cannot eliminate both, which fundamentally limits measurement precision.

To accurately evaluate wheel wear condition, this study conducts research from two aspects: high-precision monitoring of wear parameters and multi-indicator comprehensive evaluation. First, a method for wheel wear measurement using multi-dimensional laser sensors is proposed, where data from multiple sensors are fused to improve measurement precision. Second, a multi-indicator comprehensive evaluation method based on subjective and objective weights and the matter-element model is established. This model has a clear structure and simple calculation, and provides accurate and quantitative wear-grade evaluation.

2. Comprehensive Evaluation Method of Train Wheel Wear

2.1. Indicator Selection and Overall Evaluation Flow

Based on existing research on wheel wear measurement [22–24] and vehicle dynamics analysis [25–27], three core indicators are selected to evaluate the wheel wear condition, including wheel tread wear parameters flange height (*FH*), flange thickness (*FT*) and wheel diameter (*D*). These indicators are closely related to the safety and stability of train operation and they can directly reflect the overall wear degree of train wheels. In addition, they are accessible via wayside monitoring systems which ensures the engineering operability of the subsequent evaluation work. The overall evaluation process of wheel wear condition as shown in Figure 1 consists of the following key steps.

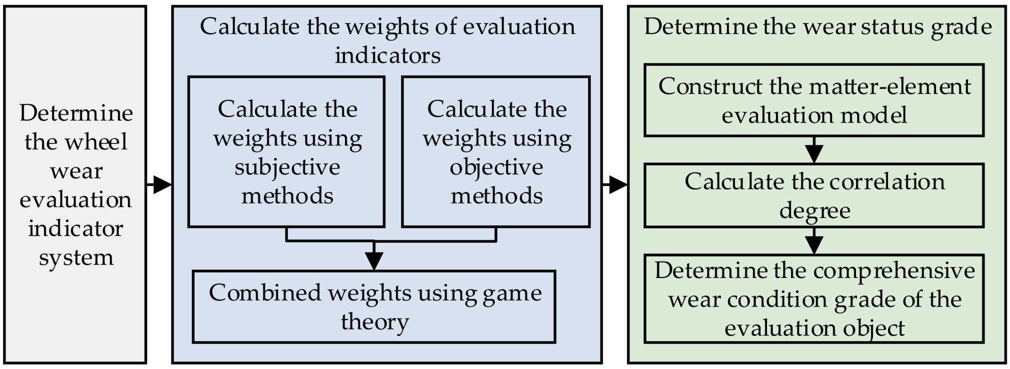

Figure 1. Overall evaluation flow of the train wheel wear comprehensive evaluation method.

First, the evaluation indicators are determined. Combined with the actual requirements of wheel wear evaluation and existing research results, the core indicators *FH*, *FT*, and *D* are selected to form an effective evaluation indicator system.

Second, the comprehensive weights of the evaluation indicators are calculated. Specifically, the Analytic Hierarchy Process (AHP) is adopted to calculate subjective weights. The Entropy Weight Method (EWM) is used to calculate objective weights. Finally, the comprehensive weights of each indicator are obtained through game theory which balances the advantages of subjective and objective weighting methods.

Finally, the matter-element evaluation model is constructed. The comprehensive correlation degree between the evaluated wheel and the preset wear condition grades is calculated through this model. Then the wear condition grade of the evaluated wheel is determined in accordance with the maximum membership principle.

2.2. Determination of Evaluation Indicator Weights

2.2.1. Subjective Weighting Based on AHP

AHP is a classic subjective weighting method that converts qualitative judgments of indicator importance into quantitative analysis, thereby solving the difficulty in directly quantifying the relative importance of wheel wear evaluation indicators and achieving more reasonable and reliable subjective weight distribution [28–30]. The key procedures for calculating subjective weights via the AHP are summarized as follows:

First, a judgment matrix is constructed by comparing the importance of each pair of indicators based on the 1–9 scale method [31]. The matrix is denoted as $A = (a_{ij})_{n\times n}$, where a_{ij} represents the importance of the i-th indicator relative to the j-th indicator, n is the number of indicators, and a_{ij} and a_{ji} are reciprocals of each other.

Second, the geometric mean of each row in the judgment matrix is calculated and normalized to obtain the subjective weight vector $w_{AHP} = (w_1, w_2, \ldots, w_{\mathrm{n}})$.

Finally, a consistency check is conducted by computing the consistency ratio CR to verify the logical rationality of the judgment matrix. The matrix is considered acceptable only if CR < 0.1; otherwise, the matrix elements need to be revised [32].

2.2.2. Objective Weighting Based on EWM

EWM is a data-driven objective weighting approach that determines indicator weights based on the degree of data dispersion, where a higher degree of dispersion corresponds to a smaller entropy value and thus a higher indicator weight, indicating a greater impact on the evaluation objective [8,30,33]. The key steps for calculating objective weights using the EWM are detailed as follows:

First, data normalization is performed to eliminate differences in dimensions and orders of magnitude among different indicators.

Second, the entropy value e_j of each indicator is calculated.

$$e_j = -\left(\sum_{i=1}^{m} f_{ij} \ln f_{ij}\right) / \ln m\,, \tag{1}$$

$$f_{ij} = y_{ij} / \sum_{i=1}^{m} y_{ij}\,, \tag{2}$$

where m represents the number of samples, f_{ij} represents the contribution of the i-th sample to the j-th indicator, and y_{ij} denotes the normalized value.

Finally, the weight of each evaluation indicator is calculated; the weight is negatively correlated with the entropy value, meaning that indicators with smaller entropy values (higher data dispersion) are assigned higher weights.

$$w_{EWM} = \left(1 - e_j\right) / \sum_{j=1}^{n} \left(1 - e_j\right), \tag{3}$$

where n is the number of indicators.

2.2.3. Combined Weights Based on Game Theory

To balance the advantages of subjective and objective weights and avoid the limitations of single weighting methods, game theory is applied to combine the weight vectors w_{AHP} and w_{EWM} calculated in the previous two sections. This method determines the optimal combination coefficients through game theory optimization, ensuring that the combined weights are effective and reasonable [11,13,30]. The key steps for calculating objective weights using game theory are detailed as follows:

First, the game theory optimization objective function is constructed based on the principle of minimum Euclidean distance between the combined weight vector and the two single weight vectors. The core goal is to minimize the deviation between the combined weight vector and the subjective and objective weight vectors.

$$min \left\| \sum_{l=1}^{2} a_l \cdot w_l - w_k \right\|_2, \tag{4}$$

where a_l represents the combination coefficients corresponding to the weight vector w_l.

Second, according to the matrix differential theory, derive the constraint conditions for the optimal combination coefficient vector $a = [a_1, a_2]^T$.

Finally, the combined weights are calculated. The obtained combination coefficient vector a is normalized, and then the normalized combination coefficients are multiplied by the corresponding subjective and objective weight vectors respectively and summed to obtain the final comprehensive combined weight vector w for each evaluation indicator.

https://doi.org/10.3390/metrology6020032

2.3. Matter-Element Evaluation Model

The matter-element evaluation model is a comprehensive evaluation method based on matter-element analysis, which accurately and intuitively determines the wear condition grades of wheels in combination with the above comprehensive weights [10,15,17].

2.3.1. Determination of Matter-Element Matrix, Classical Domain, and Joint Domain

The matter-element matrix is used to describe the evaluated object comprehensively, which expresses the evaluated wheel (denoted as N), its evaluation indicators (denoted as c) and the measured values of indicators (denoted as v) in a unified form, defined as $R = [N, c, v]$. Here, N represents the wheel to be evaluated, c corresponds to the core evaluation indicators (such as FH, FT, and D), and v is the actual measured value of each indicator.

The classical domain refers to the value range of each evaluation indicator when the evaluated wheel belongs to a specific wear grade (e.g., Excellent, Qualified, Critical, Unqualified). It is defined as $R_{oj} = [N_{oj}, c_i, x_{oij}]$.

$$R_{oj} = \begin{bmatrix} N_{oj} & c_1 & x_{o1j} \\ & c_2 & x_{o2j} \\ & c_3 & x_{o3j} \end{bmatrix} = \begin{bmatrix} N_{oj} & c_1 & (a_{o1j}, b_{o1j}) \\ & c_2 & (a_{o2j}, b_{o2j}) \\ & c_3 & (a_{o3j}, b_{o3j}) \end{bmatrix} \tag{5}$$

where N_{oj} denotes the j-th wear grade, c_i represents the i-th evaluation indicator, and xo_{ij} is the value range of the i-th indicator corresponding to the j-th wear grade.

The joint domain refers to the maximum possible value range of each evaluation indicator, which covers all possible values of the indicators in the classical domain and other potential value ranges. It is defined as $R_p = [N_p, c_i, x_{pi}]$.

$$R_{pj} = \begin{bmatrix} N_p & c_1 & x_{p1} \\ & c_2 & x_{p2} \\ & c_3 & x_{p3} \end{bmatrix} = \begin{bmatrix} N_{pj} & c_1 & (a_{p1}, b_{p1}) \\ & c_2 & (a_{p2}, b_{p2}) \\ & c_3 & (a_{p3}, b_{p3}) \end{bmatrix} \tag{6}$$

where N_p denotes the set of all possible wear condition of the wheel, and x_{pi} is the maximum possible value range of the i-th evaluation indicator, with a_{p1} and b_{p1} representing the lower and upper bounds of that range respectively.

2.3.2. Calculation of Indicator Correlation Degree

The correlation degree is employed to quantitatively measure the relevance between each indicator value of the evaluated wheel and each predefined wear grade, which is calculated based on the distance between the indicator value and the corresponding classical domain range. In this study, the correlation degree calculation is defined as follows.

$$k_{ij} = \begin{cases} 1 - \rho(v_{ij}, x_{oij}) / |x_{oij}| & v_i \in x_{oij} \\ -\rho(v_{ij}, x_{oij}) / |x_{pi}| & v_i \notin x_{oij} \end{cases}, \tag{7}$$

$$\rho(v, x) = |v - xo|, \tag{8}$$

where ρ represents the distance between the indicator value and the classical domain. Let v be the indicator value, x the classical domain, and xo the optimal value in the classical domain. Unlike the conventional centrality rule that takes the midpoint of the classical domain as the optimal value, here, xo is set to the endpoint based on the degradation trend of each indicator. For decreasing-type indicators such as D and FT, xo is taken as the upper bound of the classical domain; for increasing-type indicators such as FH, xo is taken as the lower bound of the classical domain. This adjustment better fits the degradation characteristics of each indicator.

2.3.3. Calculation of Comprehensive Correlation Degree and Wear Grade Determination

The comprehensive correlation degree $K_j(N)$ is calculated via the linear weighted summation of the correlation degree k_{ij} of each indicator and its corresponding weight w_i.

$$K_j(N) = \sum_{i=1}^{3} w_i k_{ij}, \tag{9}$$

where $K_j(N)$ denotes the comprehensive correlation degree of the evaluated wheel N with respect to the j-th wear grade, k_{ij} represents the correlation degree of the i-th indicator corresponding to the j-th wear grade, and w_i stands for the weight of the i-th indicator.

3. High-Precision Wheel Wear Measurement Method and System

To achieve high-precision online measurement of multiple key parameters that directly determine wheel wear condition, a novel measurement system fused with structured light vision sensors and displacement sensors is developed in this paper.

3.1. Definition of Wheel Wear Parameters

As shown in Figure 2, *FH* denotes the vertical distance from flange top point A to the datum point; *FT* refers to the horizontal distance from point B to the wheel inner side; and *D* represents the rolling circle diameter at the datum point. As critical indicators for wheel wear condition evaluation, the accurate measurement of these parameters is essential for reliable condition evaluation and timely maintenance. It should be clarified that work hardening, changes in surface-layer structure, wheel flats, and wheel polygons are also significant wheel issues. However, this study focuses only on the geometric parameters defined above (*FH*, *FT*, *D*), and the other factors are outside the scope of this work.

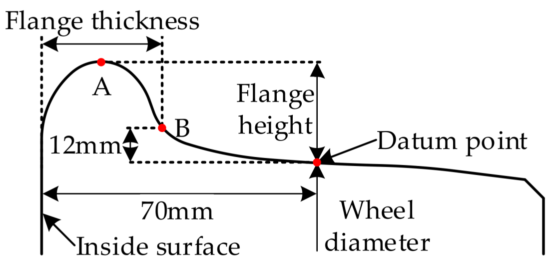

Figure 2. Schematic diagram of wheel wear parameters. Point A represents the flange top, and point B is marked as 12 mm above the datum point.

3.2. Wheel Wear Measurement Method

To achieve an accurate and reliable measurement of the key parameters, a multi-sensor fused online measurement system is developed in this study. The system design fully combines the complementary advantages of different sensing technologies. On the one hand, laser displacement sensors (LDS) feature high precision in large-range dimensional measurement and displacement measurement, which are suitable for wheel diameter measurement, but cannot obtain complete wheel profile information. On the other hand, line-structured light vision sensors (LSLVS) can reconstruct the full wheel profile effectively, but may suffer from eccentricity errors. Therefore, the synergistic fusion of LSLVS and LDS is adopted in the system design, and the data fusion is implemented in the algorithm flow to suppress measurement errors and improve overall precision. The proposed system is mainly composed of a sensor measurement unit, a position trigger unit, a data-processing unit, and a circuit-driving unit. To ensure the consistency of wear information acquired by multiple sensors and achieve high-precision measurement based on sensor fusion, an integrated layout design for multi-dimensional sensors is implemented, as illustrated in Figure 3a. Specifically, two LSLVSs are symmetrically arranged along the rail, projecting coplanar light planes along the wheel's radial direction to fully cover the tread. Meanwhile, three 1D LDS are installed outside the rail for tread scanning. As the wheel passes through the trigger unit, both types of sensors synchronously collect raw data: the LSLVS captures the light stripe images of the wheel's inner and outer contours, as shown in Figure 3b, while the LDS continuously acquires one-dimensional displacement data, as illustrated in Figure 3c. After the train passes, the sensor data are fused, and the key wear parameters are calculated to obtain the final evaluation results.

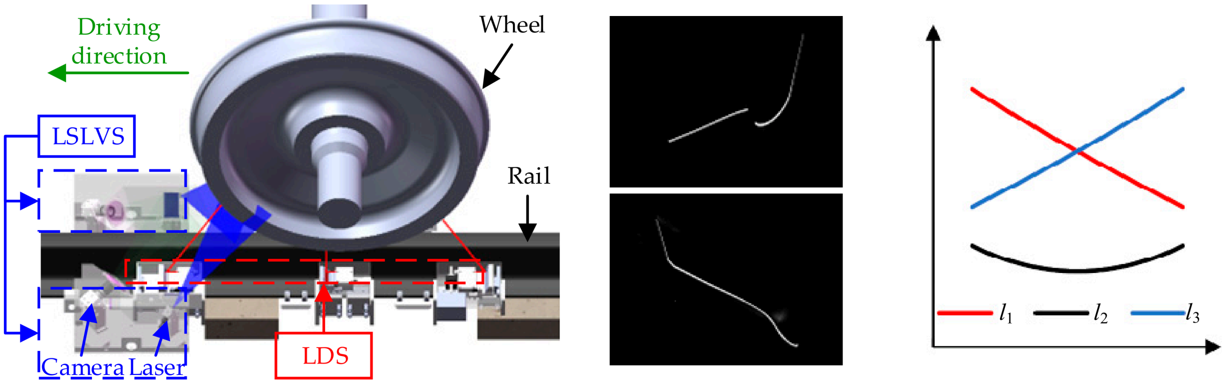

(**a**) (**b**) (**c**)

Figure 3. Sketch of wheel wear measurement system. (**a**) Sensor measurement unit, the blue and red boxes enclose the line-structured light vision sensors (LSLVS) and laser displacement sensors (LDS), respectively; (**b**) 2D images captured by LSLVSs; (**c**) distance acquired by 1D-LDSs.

3.3. Multi-Sensor Data Fusion

Based on the description of the measurement method, this section focuses on several key steps in multi-sensor data fusion measurement. First, the wheel wear parameters are initially calculated based on the measurement principle of the structured light vision sensor and the three-point diameter measurement principle. Subsequently, the core steps and mathematical model of data fusion are introduced.

3.3.1. Preliminary Calculation of Wear Parameters

The measurement principle of the structured light vision is based on the camera imaging model and light plane geometric constraints, which convert two-dimensional pixel coordinates into a three-dimensional measurement profile, as shown in Figure 4a.

Ow-XwYwZw is defined as the world coordinate system; *Oci-XciYciZci* and *Oco-XcoYcoZco* denote the coordinate systems of the inner and outer cameras, respectively; *Oii-XiiYii* and *Oio-XioYio* are the image coordinate systems of the corresponding cameras. For an arbitrary image point *pi*(*xi*, *yi*) in the image, it can be reconstructed to the world coordinate system *Pw*(*Xw*, *Yw*, *Zw*) by Equation (10) [34–36]. After reconstructing the wheel profile coordinates, *FH* and *FT* are initially calculated according to the definitions of wear parameters illustrated in Figure 2.

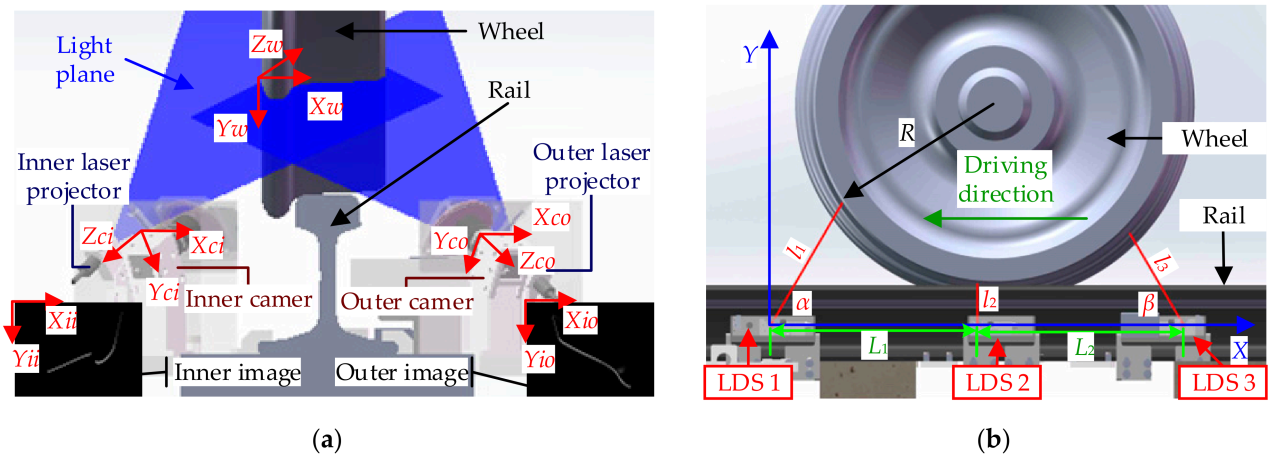

Figure 4. Principle of wheel wear measurement. (**a**) Principle of profile measurement; (**b**) principle of diameter measurement.

$$\begin{cases} aXc + bYc + cYc + d = 0 \\ Zc(xi, yi, 1)^T = McLc(Xw, Yw, Zw, 1)' \end{cases} \tag{10}$$

where (a, b, c, d) represent the coefficients of the light plane equation; Zc is a non-zero constant representing the scale factor; Mc denotes the camera intrinsic parameters; Lc represents the rigid transformation matrix of the camera coordinate system relative to the world coordinate system.

The three-point diameter measurement principle is illustrated in Figure 4b. The emission angles of the two LDSs are defined as α and β, and their distances to LDS 2 are L_1 and L_2, respectively. A two-dimensional Cartesian coordinate system is established with the left one-dimensional laser displacement sensor (LDS 1) as the origin, where X denotes the rail direction and Y represents the direction perpendicular to the rail surface, as shown in Figure 3c. The minimum value of l_2 indicates that the wheel is located directly above LDS 2. At this moment, the diameter of the measured circle is calculated according to Equation (11) [21].

$$D' = \frac{L_1^2 + l_1^2 + l_2^2 - 2L_1 l_1 cos\ \alpha - 2l_1 l_2 sin\ \alpha}{2l_1 sin\ \alpha - 2l_2} + \frac{L_2^2 + l_3^2 + l_2^2 - 2L_2 l_3 cos\ \beta - 2l_3 l_2 sin\ \beta}{2l_3 sin\ \beta - 2l_2} \tag{11}$$

Raw sensor data contain outliers, so in this study the DBSCAN clustering algorithm was used to identify and remove them, and missing values were then interpolated using least squares fitting with a second-order polynomial. DBSCAN is a density-based algorithm that uses the neighborhood radius *eps* and the minimum number of samples *min_samples* as key parameters [37]. Outliers are defined as data points in low-density regions that are not density reachable and cannot be assigned to any cluster. To determine these two parameters, the relationship between distance data and wheel position x was first modeled. The relationship of l_1 and l_3 with x is described by Equation (12), and that of l_2 with wheel running position x is given by Equation (13).

$$l_1 = xcos\ \alpha + rsin\ \alpha - \sqrt{(xcos\ \alpha + rsin\ \alpha)^2 - x^2} \tag{12}$$

$$l_2 = r - \sqrt{r^2 - (L_1 - x)^2} \tag{13}$$

Based on a sensor sampling frequency of 10 kHz and a train speed of 5 to 15 km/h, the *eps* value was set to 1.5 and *min_samples* to 20 for outlier removal. After removing the outliers, data fitting and missing value interpolation were performed. As can be seen from Equations (12) and (13), although neither equation can be simplified to a quadratic polynomial, the data curvature is very small within the limited sampling range, and the third-order and higher-order terms in the Taylor expansion of these functions are negligible. Therefore, a second-order polynomial was adopted as the model to perform least squares fitting on the monitoring data. Finally, missing values were interpolated based on the fitted polynomial, achieving outlier removal and data reconstruction.

3.3.2. Data Fusion Improves the Precision of Wear Calculation

The wheel diameter is defined as the circumference diameter at the datum point, as shown in Figure 5a, which cannot be directly measured during train operation. The red arrows denote the emission light planes of the displacement sensors. Therefore, the diameter D' calculated by Equation (11) is not the actual wheel diameter, but the circumference diameter at point P on the wheel tread. To obtain an accurate wheel diameter, further correction is required based on the profile coordinates reconstructed by the LSLVS. Thus, the actual wheel diameter D can be express as:

$$D = D' + 2\Delta r, \tag{14}$$

where Δr is calculated from the reconstructed wheel profile.

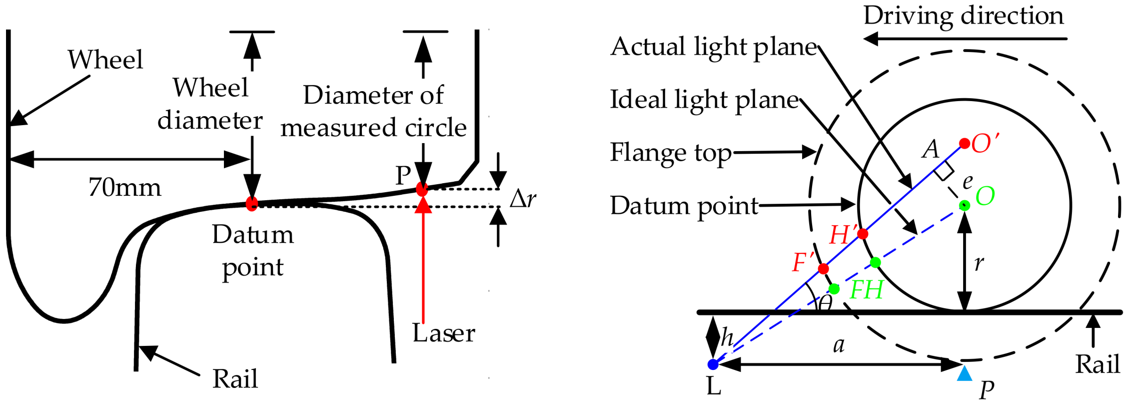

(**a**) (**b**)

Figure 5. Calculation principle of wheel wear. (**a**) Principle of diameter calculation; (**b**) principle of profile calculation.

The mathematical model for profile measurement using the vision sensor is established based on a standard wheel, as illustrated in Figure 5b. The laser L is mounted at a height h below the rail surface, and the angle between the light plane and the rail surface is θ. To ensure the light plane passes through the axle O for accurate wheel profile measurement, the trigger position P is set at a horizontal distance a from the laser, which strictly determines the moment of image capture by the camera. At this trigger instant, the light plane intersects the flange top and the datum point at points F and H, respectively, where FH corresponds to the nominal flange height of the measured wheel. However, owing to the varying diameters of actual in-service wheels, fixed trigger timing cannot guarantee that the light plane remains at the optimal position in all acquired profile images. In this case, the vertical deviation between the light plane and the actual axle is defined as e, and the measured flange height is denoted as $F'H'$. The unknown wheel diameter introduces profile distortion and degrades the accuracy of high-precision online profile measurement using only the vision sensor, which cannot compensate for such distortion.

To improve the measurement precision of wheel wear, the wheel diameter initially calculated by the 1D LDSs is adopted to correct the eccentricity error. As shown in Figure 5b, $OF = OF'$, $OH = OH' = r$. In right triangles AOH' and AOF', the following geometric constraints exist:

$$OF' = OF = r + FH = \sqrt{(F'H' + H'A)^2 + e^2}, \tag{15}$$

where $H'A = \sqrt{H'O^2 - e^2} = \sqrt{r^2 - e^2}$. As a result, the corrected FH can be expressed as:

$$FH = \sqrt{\left(F'H' + \sqrt{r^2 - e^2}\right)^2 + e^2} - r, \tag{16}$$

where the expression for the eccentricity distance e is:

$$e = (a \tan\ \theta - r - h) \cos\ \theta, \tag{17}$$

where r is the radius of the wheel to be measured.

In the multi-sensor data fusion algorithm, the tread profile reconstructed by the LSLVS and the wheel diameter measured by the LDS are mutually compensated and calibrated to improve measurement accuracy. This approach addresses the coupled deviation problem in profile and diameter measurement that cannot be resolved by a single type of sensor, thereby achieving high-precision online measurement.

To further improve measurement precision, an iterative error compensation method is proposed and its convergence is verified through simulation, with the simulation results shown in Table 1. The simulation parameters were set as follows: θ = 45°, h = 80 mm, the ideal wheel diameter was 840 mm, and a = 500 mm. Several typical wheel diameters were used in the simulation, and the wheel profile was the standard LM type. The results show that due to the positioning error of the wheel diameter, the measured diameter deviates from the true value. The simulation focuses on compensating for the effect of diameter variation on measurement error. Therefore, the diversity of tread wear depth is not considered. As a result, the deviation between the measured and true diameters is constant. Although tread wear diversity is not included, the simulation results are equally applicable to cases with tread wear.

Table 1. Iteration results at each step for convergence verification (unit: mm).

Actual Diameter	Actual Deviation e	Distorted FH	Measured Diameter	Corrected Diameter (1st)	Calculated Deviation (1st)	Corrected FH	Corrected Diameter (2nd)	Calculated Deviation (2nd)
770.000	−24.749	27.052	763.276	770.014	−24.744	27.000	770.001	−24.748
800.000	−14.142	27.016	793.276	800.004	−14.141	27.000	800.000	−14.142
840.000	0.000	27.000	833.276	840.000	0.000	27.000	840.000	0.000
880.000	14.142	27.013	873.276	880.004	14.143	27.000	880.000	14.142
910.000	24.749	27.038	903.276	910.010	24.752	27.000	910.001	24.749
1170.000	116.673	27.528	1163.276	1170.139	116.722	27.000	1170.007	116.675
1210.000	130.815	27.625	1203.276	1210.164	130.873	27.000	1210.008	130.818
1250.000	144.957	27.724	1243.276	1250.190	145.024	27.000	1250.009	144.960

During the iterative error compensation process, the wheel diameter D was first calibrated using Equations (11) and (14). The results show that the measurement error of the diameter is significantly reduced after the first calibration. Then, the eccentricity distance e was calculated using Equations (16) and (17), followed by the corrected high-precision flange height. Finally, the iteration between diameter correction and eccentricity compensation was repeated until the change in eccentricity distance e dropped below 0.1 mm. The results show that two rounds of diameter correction and one round of profile parameter correction are sufficient to meet the error compensation requirement, with the measurement errors of both diameter and flange height below 0.01 mm.

4. Experimental Verification and Discussion

To verify the effectiveness and high precision of the proposed wheel wear measurement method and comprehensive evaluation model, experiments were designed and conducted. The experiments mainly focused on two aspects: verifying the measurement precision of the wheel wear parameters (*FH*, *FT*, and *D*) and validating the reliability of the matter-element evaluation model for wheel wear condition evaluation.

4.1. Experimental Verification of Wheel Wear Measurement

The system was deployed at the train depot entry section as shown in Figure 6 to evaluate the reliability of the proposed measurement method. Each LSLVS consisted of a line-structured light laser with a wavelength of 405 nm, an industrial camera with a resolution of 1600 $\times$ 1200, and a fixed-focus lens with a focal length of 16 mm. The LSD had a sampling frequency of 10 kHz, with a resolution of 0.005 mm and an accuracy of 0.01 mm. The proposed measurement method and system were validated on a standard wheel and on real train wheels. Before the tests, each wheel was manually measured nine times using an LLJ 4A gauge and a digital wheel diameter measuring instrument (both from Liuzhou Kelu Measuring Instrument Co., Ltd., Liuzhou, China). The average of these nine measurements was taken as the reference value to evaluate the precision and repeatability of the proposed measurement system.

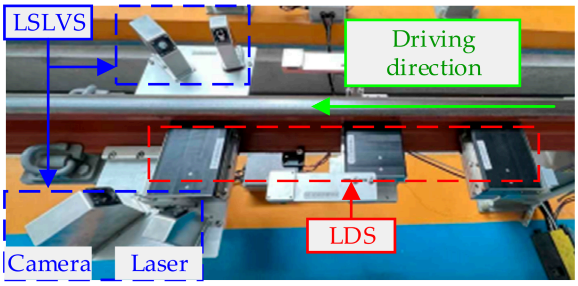

Figure 6. Physical diagram of the wheel wear measurement system, the blue and red boxes enclose the line-structured light vision sensors (LSLVS) and laser displacement sensors (LDS), respectively.

The results of multiple measurements on a standard wheelset are shown in Table 2. The standard deviations (Std) of *FH*, *FT*, and *D* were all below 0.1 mm. The mean absolute errors (MAE) were 0.04 mm, 0.07 mm, and 0.09 mm respectively, and the maximum errors (ME) were 0.07 mm, 0.12 mm, and 0.19 mm respectively. These results indicate that the measurement system achieves high precision and good repeatability.

Online measurement results for in-service train wheels are shown in Table 3, which were obtained from repeated measurements as the train passed through the measurement system at a constant speed of 5 km/h during field testing. The Std of *FH*, *FT*, and *D* are 0.09, 0.13, and 0.14 mm, respectively; the MAE are 0.15, 0.14, and 0.18 mm; and the ME are 0.24, 0.34, and 0.36 mm. These results fully meet the precision requirements of China's railway industry for online measurement systems, i.e., $\pm$1.0 mm for *D* and $\pm$0.4 mm for *FH* and *FT*, which indicates that the proposed measurement system possesses high precision and favorable repeatability.

Table 2. Measurement results of the standard wheel (unit: mm).

Measurement Number	*FH*	*FT*	*D*
1	28.07	32.32	898.20
2	28.06	32.26	898.15
3	28.03	32.30	898.01
4	28.06	32.30	898.06
5	28.01	32.23	898.02
6	28.06	32.31	898.19
7	27.99	32.22	897.94
8	28.02	32.25	898.06
Std	0.03	0.04	0.09
Mean	28.04	32.27	898.08
Manual	28.00	32.20	898.01
MAE	0.04	0.07	0.09
ME	0.07	0.12	0.19

Table 3. Measurement results of a real train wheel (unit: mm).

Measurement Number	*FH*	*FT*	*D*
1	27.80	32.58	914.49
2	27.78	32.42	914.58
3	27.84	32.45	914.71
4	27.84	32.70	914.79
5	27.67	32.36	914.44
6	27.78	32.55	914.86
7	27.63	32.42	914.79
8	27.58	32.74	914.64
Std	0.09	0.13	0.14
Mean	27.74	32.53	914.66
Manual	27.60	32.40	914.50
MAE	0.15	0.14	0.18
ME	0.24	0.34	0.36

4.2. Experimental Verification of Evaluation Model

To verify the reliability and effectiveness of the proposed wheel wear condition evaluation model, an in-depth analysis was conducted on the long-term monitoring data collected by the on-site measurement system. Installed at the railway operation site, the system continuously monitors train wheels passing through the measurement zone, with a practical measurement interval of approximately 15 days. A comprehensive evaluation was conducted on 8 sets of wear data obtained from the same wheel at different stages. These wheel wear datasets are sequentially labeled as L1, L2, . . ., L8, and the corresponding detailed data are listed in Table 4.

Table 4. Measured values of wheel wear condition indicators (unit: mm).

Indicators	L1	L2	L3	L4	L5	L6	L7	L8
FH	27.16	27.42	27.45	27.72	28.05	28.49	28.76	28.95
FT	31.95	31.92	31.87	31.75	31.76	31.61	31.67	31.49
D	838.47	837.44	837.11	836.29	836.19	835.26	834.93	834.56

According to the railway industry specifications and practical application experience, the wheel wear condition was divided into four grades: Excellent, Qualified, Critical, and

Unqualified. On this basis, the classical domain and joint domain of each wear evaluation indicator were determined. Finally, the weights of each indicator were calculated by adopting the weight calculation method described in Section 2.2. Based on discussions with experts from railway vehicle maintenance departments and the field of rail transit in universities, the judgment matrix A was constructed. The rows and columns of the matrix correspond to FH, FT, and D, respectively. The maximum eigenvalue was 3.0092, the consistency index CI was 0.0046, and the consistency ratio CR was 0.0079 (< 0.1), indicating acceptable consistency. The weights were calculated using the eigenvector method and normalized to 0.1634, 0.2970, and 0.5396 for FH, FT, and D respectively. The final combined weights and the detailed parameters of the joint domain, classical domain, and indicator weights are shown in Table 5.

$$A = \begin{bmatrix} 1 & 1/2 & 1/3 \\ 2 & 1 & 1/2 \\ 3 & 2 & 1 \end{bmatrix} \tag{18}$$

Table 5. Joint domain, classical domain, and weights of wheel wear indicators.

Indicators	Joint Domain (mm)	Classical Domain (mm)				Weights		
		Excellent	Qualified	Critical	Unqualified	Subjective Weights	Objective Weights	Combined Weights
FH	[27, 35]	[27, 29)	[29, 31)	[31, 33)	[33, 35]	0.1634	0.3304	0.2469
FT	[26, 32]	(30, 32]	(29, 30]	(28, 29]	[26, 28]	0.2970	0.3393	0.3181
D	[770, 840]	(800, 840]	(780, 800]	(775, 780]	[770, 775]	0.5396	0.3303	0.4349

Based on the determined classical domain, joint domain, and indicator weights, the indicator correlation degree of the wheel to be evaluated was calculated first, and then the comprehensive correlation degree was obtained through weighted summation. The calculation results of the indicator correlation degree and comprehensive correlation degree are shown in Tables 6 and 7, respectively. To ensure the accuracy of the evaluation, the values are retained to four decimal places in accordance with common practice.

It can be seen from Table 7 that the wheel was in the Excellent grade during the monitoring period of this stage. With the increase in operation mileage, the comprehensive correlation degree corresponding to the Excellent grade showed a gradual decreasing trend, indicating that the wear condition of the wheel gradually deteriorated as the operation mileage increased. Combined with Table 6, it can be further observed that the correlation degrees of FH, FT, and D with the Excellent grade all decreased sequentially with the increase in measurement times, which was consistent with the change trend of the comprehensive correlation degree. Among them, the flange height indicator showed the most obvious downward trend in correlation degree, indicating that flange height wear is the key factor affecting the change in wheel wear grade, which is consistent with the actual railway operation law that wheel flange wear is the main form of wheel wear.

A sensitivity analysis was performed by applying a symmetric perturbation of ±20% to each AHP weight. When one weight was perturbed, the other two were normalized proportionally to keep their sum equal to one. For each perturbation, game theory combination coefficients were recalculated to obtain new combined weights, and the wear grade and comprehensive correlation degree of every wheel sample were reevaluated. Under all perturbation conditions, the wear grade of every sample remained Excellent. The maximum changes in the comprehensive correlation degree caused by perturbing each indicator were 0.0261 for FH, 0.0161 for FT, and 0.0478 for D. All these maximum changes occurred for sample L8, where the degradation of each indicator was relatively large, but the changes were still too small to push any sample across the grade threshold. These results confirm that the proposed evaluation model is robust to reasonable variations of ±20% in the subjective AHP weights, and the evaluation conclusions remain stable.

Table 6. Correlation of wheel wear condition indicators.

Sample Number	Indicator Correlation Degree			
	Excellent	Qualified	Critical	Unqualified
L1	[0.9204, 0.9767, 0.9617]	[−0.1151, −0.3256, −0.0275]	[−0.2401, −0.4922, −0.1671]	[−0.3651, −0.3295, −0.1813]
L2	[0.7888, 0.9605, 0.9361]	[−0.0986, −0.3202, −0.0267]	[−0.2236, −0.4868, −0.1641]	[−0.3486, −0.3268, −0.1784]
L3	[0.7736, 0.9349, 0.9278]	[−0.0967, −0.3116, −0.0265]	[−0.2217, −0.4783, −0.1632]	[−0.3467, −0.3225, −0.1775]
L4	[0.6400, 0.8757, 0.9073]	[−0.0800, −0.2919, −0.0259]	[−0.2050, −0.4586, −0.1608]	[−0.3300, −0.3126, −0.1751]
L5	[0.4750, 0.8779, 0.9047]	[−0.0594, −0.2926, −0.0258]	[−0.1844, −0.4593, −0.1605]	[−0.3094, −0.3130, −0.1748]
L6	[0.2547, 0.8054, 0.8815]	[−0.0318, −0.2685, −0.0252]	[−0.1568, −0.4351, −0.1579]	[−0.2818, −0.3009, −0.1722]
L7	[0.1211, 0.8348, 0.8733]	[−0.0151, −0.2783, −0.0250]	[−0.1401, −0.4449, −0.1570]	[−0.2651, −0.3058, −0.1712]
L8	[0.0237, 0.7432, 0.8640]	[−0.0030, −0.2477, −0.0247]	[−0.1280, −0.4144, −0.1559]	[−0.2530, −0.2905, −0.1702]

Table 7. Comprehensive correlation of wheel wear condition.

Sample Number	Comprehensive Correlation Degree				Max	Grade
	Excellent	Qualified	Critical	Unqualified		
L1	0.9563	−0.1439	−0.2885	−0.2738	0.9563	Excellent
L2	0.9075	−0.1378	−0.2815	−0.2676	0.9075	Excellent
L3	0.8920	−0.1346	−0.2779	−0.2654	0.8920	Excellent
L4	0.8313	−0.1239	−0.2665	−0.2571	0.8313	Excellent
L5	0.7901	−0.1190	−0.2615	−0.2520	0.7901	Excellent
L6	0.7025	−0.1042	−0.2458	−0.2402	0.7025	Excellent
L7	0.6753	−0.1031	−0.2444	−0.2372	0.6753	Excellent
L8	0.6181	−0.0903	−0.2312	−0.2289	0.6181	Excellent

5. Discussion

Several limitations of the present work should be acknowledged. First, under complex and varying lighting conditions on site, the proposed measurement method may affect the precision and stability of light strip center extraction, which could introduce measurement errors. Second, the proposed evaluation method is data-driven and can in theory be applied to different railway lines and various vehicle operating conditions, but appropriate adjustment and validation of the relevant parameters are still required. The proposed measurement and evaluation method can be directly applied to conventional railway wheelsets, such as those used in trams and light rail vehicles, with only minor adjustments to the relevant parameters. On the other hand, the proposed evaluation method is data-driven and its idea can in principle be borrowed by roller coasters or cable transport systems like gondola lifts and ski lifts. However, these systems are subject to different operating conditions and, in some cases, involve significant safety risks. Therefore, applying the method to such systems would require accurate measurements of key indicators, as well as appropriate parameterization and experimental validation under their specific operating conditions.

The measurement system has been installed and validated at the entry section of the train depot for continuous wheel wear monitoring. For the measurement system, further improvement in accuracy and robustness can be achieved in future work by designing an adaptive algorithm for light strip center extraction. The evaluation model was developed using field monitoring data from Metro Line 3 in Shijiazhuang, China. This model is currently at the laboratory stage and will need to be tested and applied in practice with the support of relevant management departments in the future. No additional economic challenges are expected to arise from this process.

6. Conclusions

Accurate evaluation of wheel wear condition is essential for train operational safety. This study addresses the issue from two aspects. One is high-precision monitoring of wear measurement data, and the other is comprehensive evaluation of wear conditions. The main work includes the following two parts:

1. A high-precision online measurement method for train wheels is proposed based on multi-sensor data fusion. Measurement errors are compensated iteratively through data fusion to improve measurement precision.
2. A comprehensive evaluation method based on game theory combined weighting and matter-element extension theory is proposed to achieve an objective evaluation of wheel wear conditions.

The effectiveness of the proposed method was validated through experiments. First, the wheel wear measurement experiment confirmed that the method and system achieve high precision and good repeatability. For *FH*, *FT*, and *D*, Std is 0.09 mm, 0.13 mm, and 0.14 mm respectively; MAE is 0.15 mm, 0.14 mm, and 0.18 mm; and ME is 0.24 mm, 0.34 mm, and 0.36 mm. Second, the evaluation results show that the comprehensive correlation degree of the wheel remained in the Excellent grade during the monitoring period but gradually decreased, and that flange height wear is the dominant factor governing the change in wheel wear grade. This finding is consistent with actual field operation rules. In summary, this study achieves high-precision measurement and multi-indicator comprehensive evaluation of wheel wear, which can serve as a reference for wheel condition monitoring and predictive maintenance.

Author Contributions: Conceptualization and methodology, S.L. and Q.F.; software, S.L. and W.F.; validation, S.L. and Q.H. (Qixin He); investigation and data curation, S.L. and Q.H. (Qiang Han); writing—original draft preparation, S.L.; writing—review and editing, Q.F. and Q.H. (Qixin He); supervision, Q.F.; funding acquisition, Q.F. and Q.H. (Qixin He). All authors have read and agreed to the published version of the manuscript.

Funding: This work was supported in part by the Beijing Natural Science Foundation under Grant 3262008 in part by the National Natural Science Foundation of China under Grant 51935002.

Data Availability Statement: Data underlying the results presented in this paper are not publicly available at this time but may be obtained from the authors upon reasonable request.

Conflicts of Interest: Author Qiang Han was employed by the company—China Academy of Railway Sciences Corporation Limited. The author declares no conflicts of interest. The company had no role in the design of the study; in the collection, analyses, or interpretation of data; in the writing of the manuscript; or in the decision to publish the results.

References

1. Sang, H.; Zeng, J.; Qi, Y.; Mu, J.; Gan, F. Study on wheel wear mechanism of high-speed train in accelerating conditions. *Wear* **2023**, *516*, 204597. [CrossRef]
2. Tao, G.; Wang, S.; Ren, D.; Li, J.; Wen, Z. Understanding and treatment of severe flange wear of metro train wheels. *Veh. Syst. Dyn.* **2022**, *61*, 2415–2431. [CrossRef]
3. Bosso, N.; Magelli, M.; Zampieri, N. Simulation of wheel and rail profile wear: A review of numerical models. *Railw. Eng. Sci.* **2022**, *30*, 403–436. [CrossRef]
4. Zhang, H.; Wei, X.; Guan, Q.; Zhang, W. Joint maintenance strategy optimization for railway bogie wheelset. *Appl. Sci.* **2022**, *12*, 6934. [CrossRef]

5. Wang, Q.; Li, D.; Zeng, J.; Peng, X.; Wei, L.; Du, W. A diagnostic method of freight wagons hunting performance based on wayside hunting detection system. *Measurement* **2024**, *227*, 114274. [CrossRef]
6. Wang, Q.; Gao, H.; Shi, H.; Wu, S.; Li, D.; Zeng, J. Real-time detection of vehicle hunting performance using a newly proposed evaluation indicator: Methodology and experimental validation. *Measurement* **2025**, *256*, 118163. [CrossRef]
7. Dai, X.; Qu, S.; Huang, C.; Wu, P. The determination of limit wheel profile for hunting instability of railway vehicles using stacking feature deep forest. *Eng. Appl. Artif. Intell.* **2023**, *125*, 106732. [CrossRef]
8. Li, Y.; Deng, J.; Wang, Y.; Liu, H.; Peng, L.; Zhang, H.; Liang, Y.; Feng, Q. The condition evaluation of bridges based on fuzzy BWM and fuzzy comprehensive evaluation. *Appl. Sci.* **2025**, *15*, 2904. [CrossRef]
9. Wang, X.; Yang, J.; Wang, J.; Wang, Y.; Xu, G. An incentive factor-based dynamic comprehensive evaluation on a high-speed railway track. *Appl. Sci.* **2020**, *10*, 5546. [CrossRef]
10. Zhang, G. Typical process capability analysis of small-batch production based on fuzzy matter-element. *Chin. J. Mech. Eng.* **2015**, *51*, 116–122. [CrossRef]
11. Yi, L.; Zhao, J.; Yu, W.; Long, G.; Sun, H.; Li, W. Health status evaluation of catenary based on normal fuzzy matter-element and game theory. *J. Electr. Eng. Technol.* **2020**, *15*, 2373–2385. [CrossRef]
12. Han, F.; Liu, Z.; Wang, C. Research on a comfort evaluation model for high-speed trains based on variable weight theory. *Appl. Sci.* **2023**, *13*, 3144. [CrossRef]
13. Tang, J.; Wang, D.; Ye, W.; Dong, B.; Yang, H. Safety risk assessment of air traffic control system based on the game theory and the cloud matter element analysis. *Sustainability* **2022**, *14*, 6258. [CrossRef]
14. Shu, J.; Ma, H.; Ding, W.; Jin, Z. Improved evidence fusion theory for the safety assessment of prestressed concrete bridges. *Buildings* **2024**, *14*, 1144. [CrossRef]
15. Li, Q.; Fan, C. Evaluation of hydraulic-tunnel-lining durability based on ANP and cloud-model-improved matter-element theory. *Sustainability* **2022**, *14*, 11801. [CrossRef]
16. Zhang, X.; Wu, Z.; Wang, H.; He, C.; Zhang, F.; Zhou, Y. Urban meteorological drought comprehensive index based on a composite fuzzy matter element-moment estimation weighting model. *iScience* **2024**, *27*, 110798. [CrossRef]
17. Peng, H.; Chen, Y.; Shangguan, L.; Zhou, S.; Li1, Y.; Wang, Q. Evaluation of urban rail transit system planning based on integrated empowerment method and matter-element model. *Sustainability* **2025**, *17*, 4569. [CrossRef]
18. Zeng, Y.; Song, D.; Zhang, W.; Zhou, B.; Xie, M.; Tang, X. A new physics-based data-driven guideline for wear modelling and prediction of train wheels. *Wear* **2020**, *456–457*, 203355. [CrossRef]
19. Ran, Y.; He, Q.; Feng, Q.; Cui, J. High-accuracy on-site measurement of wheel tread geometric parameters by line-structured light vision sensor. *IEEE Access* **2021**, *9*, 52590–52600. [CrossRef]
20. Pan, X.; Liu, Z.; Zhang, G. On-site reliable wheel size measurement based on multisensor data fusion. *IEEE Trans. Instrum. Meas.* **2019**, *68*, 4575–4589. [CrossRef]
21. Zheng, F.; Zhang, B.; Gao, R.; Feng, Q. A high-precision method for dynamically measuring train wheel diameter using three laser displacement transducers. *Sensors* **2019**, *19*, 4148. [CrossRef] [PubMed]
22. Chen, Y.; Li, Y.; Niu, G.; Zuo, M. Offline and online measurement of the geometries of train wheelsets: A review. *IEEE Trans. Instrum. Meas.* **2022**, *71*, 3523915. [CrossRef]
23. Liu, F.; Liang, L.; Hou, C.; Xu, G.; Liu, D.; Wang, L.; Chen, X.; Du, H. Measurement and evaluation of wheel profiles of a rail vehicle on an underfloor wheelset lathe. *Meas. Sci. Technol.* **2022**, *33*, 095010. [CrossRef]
24. Song, Z.; Guo, Z.; Zhou, F.; Tan, H.; Wang, X.; Zhang, P. Structured-light vision measurement approach for geometric parameters of wheelset under variable re-profiling working conditions. *IEEE Trans. Instrum. Meas.* **2025**, *74*, 5034212. [CrossRef]
25. Li, H.; Li, L.; Yu, X.; Li, Z.; Sun, Y. Research on the influence of time-varying wear of wheel-rail profile on vehicle dynamic response. *Tribol. Int.* **2024**, *200*, 110095. [CrossRef]
26. Fang, C.; Ding, Y.; Yan, H.; Chen, J.; Zhou, W.; Meng, X. Prediction and analysis of wheel flange wear on small curved track considering wheel-rail conformal and lubricated contact. *Wear* **2024**, *558*, 205569. [CrossRef]
27. Muhamedsalih, Y.; Tucker, G.; Stow, J. Optimisation of wheelset maintenance by using a reduced flange wear wheel profile. *Proc. Inst. Mech. Eng. Part F-J. Rail Rapid Transit* **2022**, *237*, 253–265. [CrossRef]
28. Saaty, T.L. A scaling method for priorities in hierarchical structures. *J. Math. Psychol.* **1977**, *15*, 234–281. [CrossRef]
29. Zhang, J.; Li, M.; Zhang, J.; Yu, Y.; Liu, H.; Gao, H. A framework for condition assessment of communication tower with inspection data in Heilongjiang province, China. *Structures* **2025**, *75*, 108710. [CrossRef]
30. Zhang, G.; Liu, G.; Lu, Z.; Yan, C.; Xu, L.; Gao, Q.; Zhou, Y. Evaluation method for health state of highway tunnel structure based on adaptive comprehensive weighting. *Eng. Fail. Anal.* **2024**, *163*, 108597. [CrossRef]
31. Kim, J.; Kim, C.; Kim, G.; Kim, I.; Abbas, Q.; Lee, J. Probabilistic tunnel collapse risk evaluation model using analytical hierarchy process (AHP) and delphi survey technique. *Tunn. Undergr. Space Technol.* **2022**, *120*, 104262. [CrossRef]
32. Xiao, K.; Tamborski, J.; Wang, X.; Feng, X.; Wang, S.; Wang, Q.; Lin, D.; Li, H. A coupling methodology of the analytic hierarchy process and entropy weight theory for assessing coastal water quality. *Environ. Sci. Pollut. Res.* **2022**, *29*, 31217–31234. [CrossRef]

33. Jiang, W.; Wu, J.; Yang, Y.; Li, X.; Zhu, H. Health evaluation techniques towards rotating machinery: A systematic literature review and implementation guideline. *Reliab. Eng. Syst. Saf.* **2025**, *260*, 110924. [CrossRef]
34. Chen, X.; Sun, J.; Liu, Z.; Zhang, G. Dynamic tread wear measurement method for train wheels against vibrations. *Appl. Opt.* **2015**, *54*, 5270–5280. [CrossRef]
35. Liu, S.; He, Q.; Fu, W.; Du, B.; Feng, Q. Multi-scale adaptive light stripe center extraction for line-structured light vision based online wheelset measurement. *Sensors* **2026**, *26*, 600. [CrossRef]
36. He, Q.; Liu, S.; Fu, W.; Zhang, Z.; Feng, Q. High-accuracy on-line wayside wheelset size measurement based on multi-dimensional laser information fusion. *Measurement* **2025**, *254*, 117930. [CrossRef]
37. Wang, C.; Ji, M.; Wang, J.; Wen, W.; Li, T.; Sun, Y. An improved DBSCAN method for LiDAR data segmentation with automatic eps estimation. *Sensors* **2019**, *19*, 172. [CrossRef] [PubMed]

https://doi.org/10.3390/metrology6020032